Title

Atomic force microscopy shows connexin26 hemichannel clustering in purified membrane fragments.

Journal

Biochemistry, 53(47)

ISSN

0006-2960

Authors

Meckes, Brian
Ambrosi, Cinzia
Barnard, Heather
et al.

Publication Date

2014-12-01

DOI

10.1021/bi501265p

Peer reviewed

BIOCHEMISTRY
including biophysical chemistry & molecular biology

Article

pubs.acs.org/biochemistry

Atomic Force Microscopy Shows Connexin26 Hemichannel Clustering in Purified Membrane Fragments

Brian Meckes,[†] Cinzia Ambrosi,[‡] Heather Barnard,[†] Fernando Teran Arce,[†,§] Gina E. Sosinsky,*[,‡,∥] and Ratnesh Lal*[,†,§,⊥]

[†]Department of Bioengineering, [‡]National Center for Microscopy and Imaging Research, [§]Department of Aerospace and Mechanical Engineering, [∥]Department of Neurosciences, and [⊥]Materials Science Program, University of California San Diego, 9500 Gillman Drive, La Jolla, California 92093, United States

ABSTRACT: Connexin proteins form hexameric assemblies known as hemichannels. When docked to form gap junction (GJ) channels, hemichannels play a critical role in cell−cell communication and cellular homeostasis, but often are functional entities on their own in unapposed cell membranes. Defects in the Connexin26 (Cx26) gene are the major cause of hereditary deafness arising from dysfunctional hemichannels in the cochlea. Structural studies of Cx26 hemichannels properly trafficked and inserted in plasma membranes, including their clustering that forms a plaque-like feature in whole gap junctions, are limited. We used atomic force microscopy (AFM) to study the surface topography of Cx26 hemichannels using two different membrane preparations. Rat Cx26 containing appended carboxy terminal V5 and hexahistidine tags were expressed in baculovirus/Sf9 cell systems. The expressed Cx26 proteins form hemichannels in situ in Sf9 cells that were then purified either as (1) Sf9 membrane fragments containing Cx26 hemichannels or (2) solubilized hemichannels. The latter were subsequently reconstituted in liposomes. AFM images of purified membrane fragments showed clusters of protein macromolecular structures in the membrane that at higher magnification corresponded to Cx26 hemichannels. Hemichannels reconstituted into DOPC bilayers displayed two populations of channel heights likely resulting from differences in orientations of inserted hemichannels. Hemichannels in the protein rich portions of purified membranes also showed a reduced channel height above the bilayer compared to membranes with reconstituted hemichannels perhaps due to reduced AFM probe access to the lipid bilayer. These preparations of purified membranes enriched for connexin hemichannels that have been properly trafficked and inserted in membranes provide a platform for high-resolution AFM imaging of the structure, interconnexon interactions, and cooperativity of properly trafficked and inserted noncrystalline connexin hemichannels.

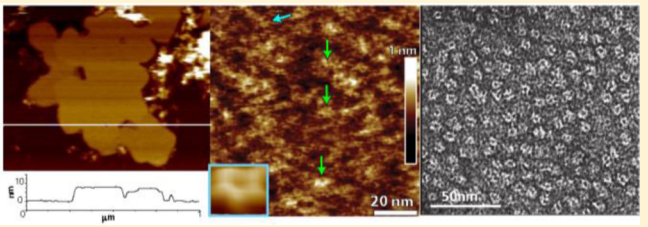

The connexin (Cx) family of proteins is a group of ubiquitously expressed transmembrane proteins with high conservation of structure and genetics between species. Cx proteins form assemblies in the cell plasma membranes known as hemichannels (or connexons) consisting of 6 Cx subunits. Hemichannels on apposing cells dock together to form gap junction (GJ) channels that facilitate cell−cell communication through transport of ions, metabolites, and other small molecules between neighboring cells. Undocked hemichannels have been shown to be present in cells[1] and have demonstrated ionic conductance states as well as metabolite, dye, and Ca^{2+} transfer.[2−6] Gating of hemichannel and GJ channel activity is regulated by many factors, including Ca^{2+}, pH, phosphorylation, and redox state.[7−10] During oxidative stress, hemichannels lose regulation leading to unchecked hemichannel opening that ultimately results in cell death.[11,12] To better understand the structures that determine the activity of hemichannels, imaging of these structures within membrane environments must be performed.

Previous imaging has extensively revealed subnanometer resolution 3-D structures of Cx hemichannels and GJ channels using X-ray crystallography, X-ray diffraction, and electron crystallography.[13−17] All are based on crystallized or quasi-crystallized arrangements of GJ channels. In contrast, atomic force microscopy (AFM) allows high resolution imaging of noncrystalline biological samples in aqueous, nonstatic environments. Previously, high resolution AFM images of the extracellular surface of Cx26 hemichannels derived from force dissected quasi-crystalline dodecameric channels showed fine details and conformational changes in response to either Ca^{2+} or low pH.[18,19] However, native undocked hemichannels exist in noncrystalline clusters and populations are often diffuse in the native membrane environment. The open and closed states of Cx43 and Cx40 hemichannels reconstituted in lipid bilayers contained noncrystalline patches of membrane bound hemichannels that showed Ca^{2+} induced conformational changes when exposed to high Ca^{2+} concentrations.[20,21] However, reconstitution of hemichannels does not always mimic the native composition of eukaryotic plasma membranes and can have widely varying protein densities. It also lacks the cellular

Received: October 8, 2014
Published: November 3, 2014

   dx.doi.org/10.1021/bi501265p | *Biochemistry* 2014, 53, 7407−7414

control for correct, directed trafficking and insertion of hemichannels into membranes. In order to overcome this limitation, we have utilized purified membrane fragments from cells expressing Cx26 hemichannels at high levels.

In this study, we focused on imaging of noncrystalline Cx26 hemichannels, which allows for easier high resolution imaging due to their shorter cytoplasmic C-terminal domain. Connexins share a common topology with high sequence conservation in their N-terminus, transmembrane domains, and extracellular loops. Connexins larger than 40 kDa have C-termini that contain as much mass as the transmembrane and extracellular domains combined. The amino acid sequences of the connexin C-termini vary considerably, with each containing critical regulatory regions essential to channel function. The cytoplasmic domains are very flexible and probably act similarly to intrinsically disordered proteins.[22] This inherent flexibility has made imaging high resolution structural details difficult.

Here, we report AFM imaging of noncrystalline Cx26-V5-His_6 hemichannels expressed through baculovirus infected Sf9 insect cells. We take advantage of the fact that connexins readily form hemichannels or channels in the membranes of baculovirus infected Sf9 cells that allow for purification of milligram quantities of hemichannels. It is important to emphasize that we studied Cx26 not only for its short C-terminus, but also because genetic defects in the human gjbeta2 gene (Cx26) are the leading cause of the most common type of hereditary congenital hearing impairment due to altered structure that can prevent docking of hemichannels or alter trafficking of molecules through the channels.[23−25] We used purified membrane fragments of Sf9 cells containing Cx26 hemichannels to image the structure of dispersed hemichannels in membranes and compared these to images of purified hemichannels reconstituted in 1,2-dioleoyl-*sn*-glycero-3-phosphatidylcholine (DOPC) liposomes. The hemichannels expressed in the purified membrane fraction of cells showed regions of clustering. The protrusion of hemichannels above the membrane was reduced in comparison to the reconstituted hemichannel preparations.

EXPERIMENTAL PROCEDURES

Baculovirus Expression of Hemichannels in Insect Cells. Rat Cx26-V5-His_6 (NCBI Reference Sequence: NM_001004099.1) was expressed through cloning into a pBlueBac baculovirus system as previously described in Beahm et al.[26] Baculoviruses were generated and used for subsequent infection of *Spodoptera frugiperda* (Sf9) cells. The techniques for applying this to expression of connexin hemichannels have been described extensively in our previous publications.[24,26−28]

Insect Cell Membrane Purification. In Sf9 cells, Cx26 readily forms channels and hemichannels in the plasma membrane and internal membranes. Hemichannel expressing Sf9 cell membranes were purified using our published protocol.[27]

Hemichannel Purification. Solubilized hemichannel proteins were purified from baculovirus expression in Sf9 cells utilizing the hexahistidine tag for affinity purification, as we have previously reported.[13,24,26,27,29]

Reconstitution of Hemichannels. 1,2-Dioleoyl-*sn*-glycero-3-phosphatidylcholine (DOPC) lipids (Avanti Polar Lipids, Alabaster, AL) (5 mg/mL) in chloroform were vacuum-dried. The lipids were then resuspended in 150 mM KCl, 10 mM HEPES, 1.8 mM $MgCl_2$ buffer (pH 7.5) (final DOPC concentration of 0.8 mg/mL) with *n*-octyl-β-D-glucoside (OG) (5 mg/mL). The mixture was briefly vortexed followed by 15 min of sonication to create mixed detergent−lipid liposomes. Purified Cx26-V5-His_6 hemichannels in elution buffer were added at 1:200 to the liposomes. The mixture was sonicated for 2 min and then gently mixed for 1 h at 4 °C. The detergent was removed to create proteoliposomes by treatment with Biobeads (Bio-Rad Laboratories, Hercules, CA) (0.1 g/mL) twice for 2 h or overnight at 4 °C.

AFM Imaging of Hemichannels. Imaging was performed on a multimode atomic force microscope with a Nanoscope IIIA or Nanoscope V controller utilizing a fluid cell (all from Bruker, Santa Barbara, CA). A TRP300A cantilever (Asylum Research, Santa Barbara, CA) with spring constants 0.02 N/m (contact mode) and 0.08 N/m (tapping mode) was used for all imaging. For imaging of the reconstituted hemichannels, proteoliposomes were deposited on freshly cleaved mica (20 μL) and allowed to attach for 30 min. The sample was heated for 5 min at 37 °C to induce liposomal fusion. The sample was then rinsed 3 times with "imaging buffer" (10 mM HEPES, 1 mM PMSF, pH 7.4) and then imaged in appropriate buffer. For imaging of membrane fragments containing hemichannels, 20 μL of the Sf9 membrane suspension was deposited on mica. The mica had been incubated with "pretreatment buffer" (10 mM HEPES, 1 mM PMSF, pH 8.5) that we found reduced rolling or folding of the flexible membranes. After a 10 min incubation to allow absorption of the membrane fragments onto the mica, samples were rinsed twice in "pretreatment buffer" and then rinsed in an imaging buffer (10 mM HEPES, 1 mM PMSF, pH 7.4) just prior to imaging in the buffer. Images were taken with raster scans at rates between 1 and 2 Hz for tapping mode images and 5−10 Hz for contact mode. The samples were imaged with scan sizes ranging from 10 μm × 10 μm to 100 nm × 100 nm. High resolution images were taken with pixel sizes less than 1 nm.

Gel and Western Blots. Isolated membranes and purified hemichannels were checked for purity by gel staining for protein bands and Western blots. Between 5 and 15 μL of sample were mixed with 2x Novex Tricine SDS Buffer (Life Technologies, Carlsbad, CA LC1676) in the presence of 5% BME. The samples were boiled for 10 min and loaded on 4−20% SDS-PAGE gel for electrophoresis. For protein staining, the gels were then fixed and stained with SYPRO Ruby solution (Life Technologies S-12000) overnight. For Western blots, the gels were transferred to PVDF membrane using the iBlot dry blotting system. Band detection was performed using the Li-Cor Odyssey Fc (Li-Cor Biosciences, Inc., Lincoln, NE) after reaction with ECL Luminata Forte (EMD Millipore, Billerica, MA).

Analysis of Lipid Bilayers Containing Cx26 Hemichannels. Lipid bilayers were deposited on mica substrates following the procedure described for preparing reconstituted hemichannels for AFM imaging. The mica substrate was broken into pieces and put into 1.5 mL Eppendorf tubes. Twenty microliters of loading sample buffer, Novex Tricine SDS Sample Buffer (Life Technologies) mixed with 5% BME, was added to the tubes. The tubes were then boiled for 10 min in a thermo block and loaded on an SDS gel PAGE 4−20% acrylamide for Western blotting. Band detection was performed with an anti-His primary antibody (Life Technologies) and an anti-mouse fluorescent secondary antibody and imaged by an Odyssey Fc instrument.

Electron Microscopy. Samples of isolated membranes (5 μL) were applied to carbon coated grids, rinsed with ddH_20,

negatively stained with 2% uranyl acetate, and then air-dried. Electron microscopy (EM) was performed by using a 120 kV FEI Tecnai transmission electron microscope (FEI, Hillsboro, OR). Images were acquired at 30 000 magnification using a TVIPS TemCam-F224 2k × 2k CCD camera (TVIPS, Gauting, Germany).

Data Analysis of AFM Data. Images were initially processed using the Nanoscope Analysis 1.4 software package (Bruker, Santa Barbara, CA) to apply image flattening to correct for piezotube motion artifacts and a low pass Gaussian filter to eliminate electrical and mechanical noise. We used the Origin Pro 7.5 software package (OriginLabs, Northampton, MA) to determine the mean bilayer heights by plotting a histogram of the pixel heights and then fitting Gaussian curves to each histogram to determine the peak and standard deviation of the distributions. All subsequent statistical analyses were also performed with Origin Pro 7.5. All statistical values are reported as mean ± standard deviation.

RESULTS

Baculovirus Sf9 infected cells are an excellent system for expressing eukaryotic proteins in quantities typically required for structural biology experiments. In the case of connexins, the protein subunits oligomerize to form hexamers or dodecamers in situ that have been shown to be structurally and functionally the same as proteins expressed exogenously in other cells or in native systems.[3] The resulting hemichannels were either (1) recovered in the membrane fragment fraction of the expressing cells or (2) solubilized from cell membranes and purified as detergent stabilized hemichannels.

EM and Biochemical Validation of Purified Membranes Containing Hemichannels. Protocols for purifying GJs depend on the fact that the intrinsic protein to lipid ratio is high in these membrane specializations and increased after detergents extractions, making density gradient separation methods effective for isolating highly enriched fractions containing GJs. Hemichannel-containing membranes also had a high protein to lipid ratio, and thus, these same methods yield good results for our hemichannel membranes as well.[30] To purify membranes containing Cx26 hemichannels, partially disrupted membranes were collected utilizing a membrane selective sucrose gradient followed by washing with detergents. Because density gradient fractionation is selective for overall density but not for protein composition, we concentrated and further enriched membrane fragment fractions containing high density expressions of Cx26 by taking advantage of the genetically appended His_6 tag binding to Ni-NTA beads for affinity separation.

Following successful purification of membrane fragments containing hemichannels, the membrane fragments were imaged with EM (Figure 1). Electron micrographs of uranyl acetate stained purified membrane fragments show the presence of hemichannel structures (Figure 1B) whose appearance in these projection images we previously referred to as "doughnut-like". Gel staining and Western blotting of these membranes confirmed the presence of Cx26 proteins in the purified membrane fraction (Figure 1C,D).

Membranes from uninfected Sf9 cells were imaged as a negative control. In this case, we did not use a Ni-NTA affinity purification step because there was no His_6 tag expressed in this sample. No doughnut-like structures were seen in these uranyl-acetate stained membranes. Furthermore, only trace amounts of proteins were found within these membranes (Figure 1C) and none of these very faint bands were identified as Cx26 in matched Western blots (Figure 1D).

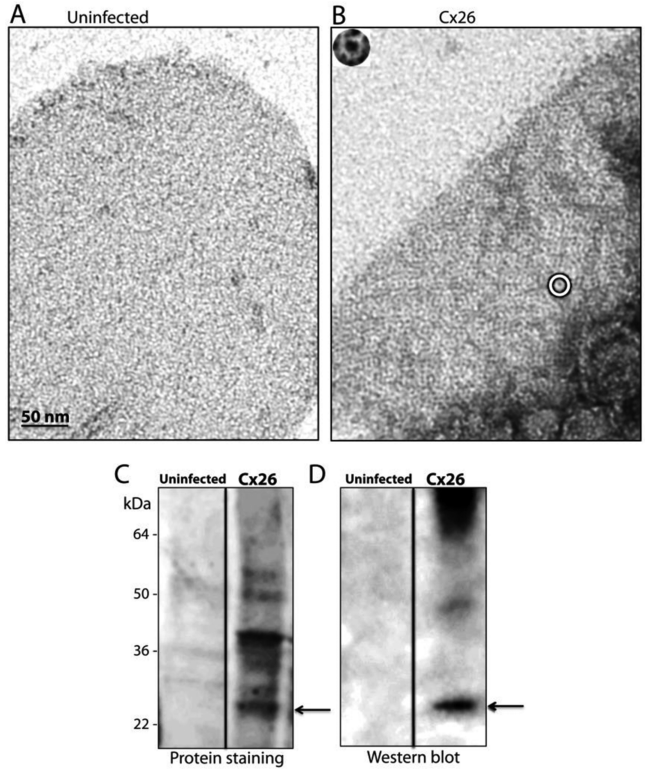

Figure 1. EM and biochemical characterization of purified membranes from Cx26 expressing Sf9 cells. (A,B) Representative electron micrographs of uranyl acetate stained purified membranes without Cx26 expression (uninfected) (A) and with Cx26 expression (B). The inset in (B) shows a "doughnut-like" hemichannel structure present in the membrane (circled in white). (C,D) Protein staining (C) and Western blots (D) confirmed the presence of Cx26 in these preparations, while a similar analysis of uninfected cells did not contain any Cx26 bands. Oligomeric forms of Cx26 in the sample are due to protein aggregation when running the gel and are over-emphasized in the Western blot.

AFM of Purified Membrane Fragments with Cx26 Hemichannels. Purified membranes of Sf9 cells expressing Cx26 were deposited onto freshly cleaved mica and imaged in aqueous buffer (Figure 2). Membrane fragments greater than 500 nm in diameter were further imaged at high resolution to examine the Cx26 structure. Smaller bilayers were more susceptible to membrane disruption when imaged and thus, high resolution images of these proved difficult to record. Since the AFM *z*-resolution is very accurate, it was easy to identify single layers from double layers or folded membranes; heights greater than 12 nm were most likely either due to the presence of GJs (double membranes containing two docked hemichannels) or due to the superposition of hemichannel layers that occurred during sample deposition, respectively. Some of the bilayer fragments displayed inhomogeneity throughout the surface as cross section showed distinct clusters with two populations of bilayer thickness (Figure 2A–D), while other fragments showed more homogeneous height profiles (Figure 2E). The membrane in Figure 2E contained small protein-rich islands in a lipidic membrane. The height difference between the two populations in the membranes exhibiting multiple heights was measured by first finding the pixel height in localized regions (outlined in Figure 3) and then plotting the

dx.doi.org/10.1021/bi501265p | *Biochemistry* 2014, 53, 7407–7414

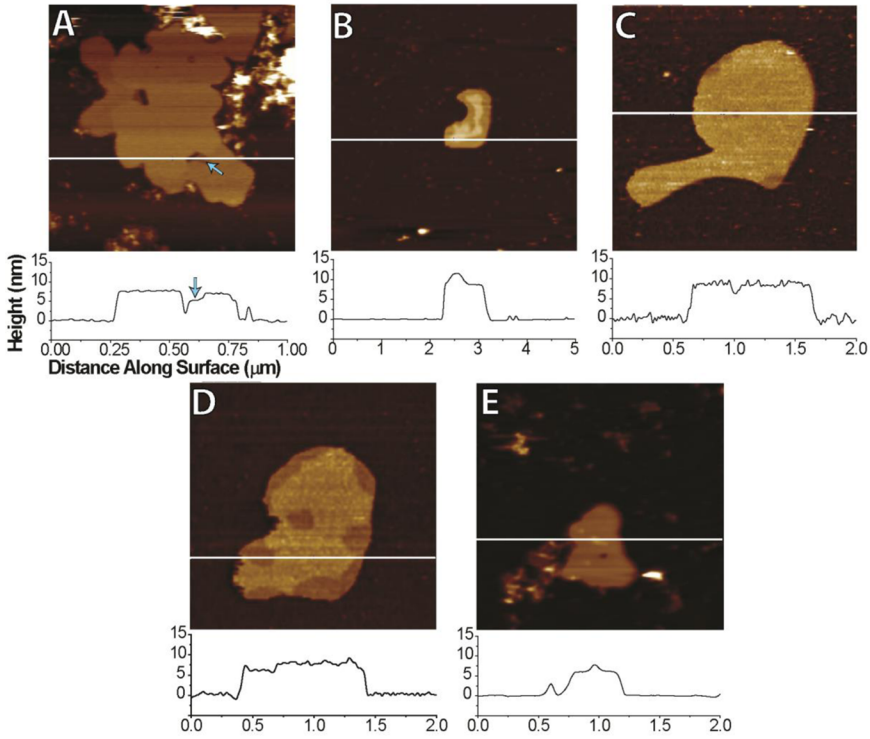

Figure 2. AFM images of purified membrane fragments containing Cx26 hemichannels. (A–E) Purified Cx26 hemichannel containing fragments were deposited on the mica substrate and imaged. Shown here are several AFM images of large (>500 nm) purified membrane fragments containing Cx26 hemichannels. The height profile section of the membrane (white line) is shown below its corresponding image. Note the difference in thickness between the purely lipidic domains and hemichannel containing regions. In (A), the membrane shows three heights possibly due to proteins with different orientations and lipidic regions (arrow).

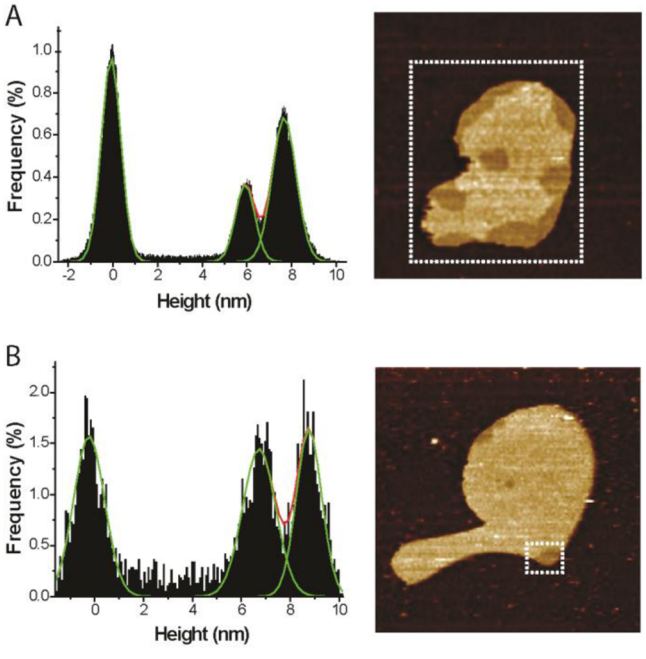

Figure 3. Height histograms for two representative purified membrane fragments containing hemichannels. (A) Histogram of the distribution of heights shows two populations of membrane height for a membrane fragment (boxed on right). (B) Height histogram of a small portion of a membrane (boxed on right) also displays two membrane heights. Gaussian curves were fit to the histogram data.

heights as a histogram (Figure 3). Gaussian distributions fit to each histogram better quantified the height of the two bilayer populations. The height of the bilayers in the lower population was 5.9 ± 1.6 nm, which were not statistically different from the heights measured for the homogeneous membrane population 5.2 ± 0.6 nm (t test, $p > 0.05$). The step height difference between the lipidic and protein rich regions in the membranes was determined to be 1.8 ± 0.4 nm ($n = 6$ measurements). The regions of the bilayer displaying an increased thickness, we believe, contain greater concentrations of hemichannels. Magnified images of the membrane patches showed the presence of hemichannels dispersed throughout the membranes (Figure 4). The protrusion height of these hemichannels above

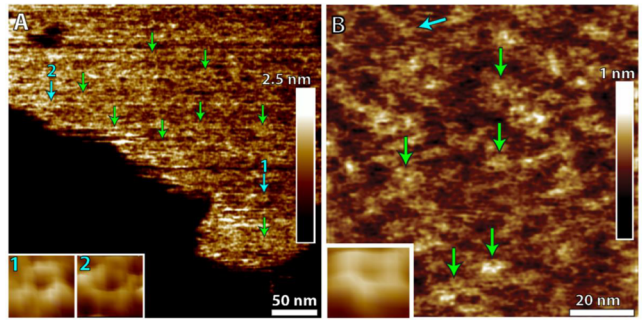

Figure 4. AFM images of purified membrane fragments containing Cx26 hemichannels. (A) Height image of a membrane fragment with disordered hemichannels (green arrows). Insets contain selected hemichannels that have been enlarged (cyan arrows numbered on figure). (B) High resolution height image of a membrane fragment containing many Cx26 hemichannels (green arrows). Inset shows an enlarged 3D image of a hemichannel present in the membranes (indicated by cyan arrow).

dx.doi.org/10.1021/bi501265p | *Biochemistry* 2014, 53, 7407–7414

the surrounding protein and lipid was limited to 0.4 ± 0.2 nm (n = 18). The dense packing and overall increased height in the step regions most likely contributed to this lower protrusion height of the hemichannels.

EM and Biochemical Validation of Purified Detergent Stabilized Hemichannels. In our comparison of two ways of making hemichannel-containing membranes, we used purified hemichannels collected from baculovirus membranes via full membrane disruption and detergent solubilization. The DoDM detergent stabilizes membrane proteins to allow them to retain their structure and prevent aggregation. Detergent stabilized hemichannels were imaged with EM with uranyl acetate as the contrast agent (Figure 5). These channels were present in "doughnut-like" structures typical of hemichannels. Protein staining and Western blotting of SDS-PAGE confirmed the presence of Cx26 hemichannels as the primary constituent of the purified lysate. This evidence confirmed the successful purification of hexamer hemichannels for eventual reconstitution and imaging with AFM (Figure 4).

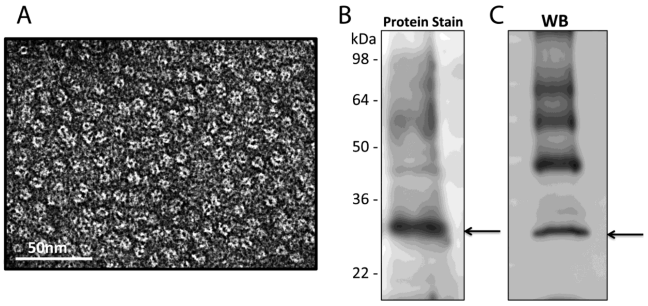

Figure 5. EM and biochemical characterization of purified hemichannels from Cx26 expressing Sf9 cells. (A) Electron micrograph of a uranyl-acetate stained Cx26 hemichannel preparation typically used for reconstitution into DOPC vesicles. (B) Staining an SDS PAGE with Sypro Ruby for protein content confirmed the presence of a strong Cx26 band in this sample that is further verified by Western blotting (C). Oligomeric forms of Cx26 in the sample are due to protein aggregation when running the gel and are overemphasized in the Western blot.

AFM Of Cx26 Hemichannels Reconstituted into Lipid Membranes. As we did for the isolated membrane preparations, we compared hemichannel containing reconstituted membranes to ones prepared without hemichannels. Prior to imaging bilayers formed by the proteoliposomes, bilayers formed from liposomes containing only DOPC were imaged to measure their size, heights, and surface structure. We used DOPC for hemichannel reconstitution because these lipids have a very low phase transition temperature (−17 °C), which facilitates the facile formation of bilayers, as has been previously documented.[13,20,21,29] These lipid bilayers showed a step height of ∼5.5 nm (data not shown), consistent with dimensions from the literature on DOPC bilayer thickness.[31]

Next, we imaged Cx26 hemichannels reconstituted into DOPC lipid bilayers. Purified Cx26 hemichannels were reconstituted in mixed DOPC/OG liposomes. The DoDM and OG were subsequently removed with polystyrene beads. The DOPC proteoliposomes were deposited on mica and imaged with AFM in the presence of calcium free buffers to ensure open configurations of the hemichannels (Figure 6). The presence of hemichannel proteins in the liposomes was confirmed by Western blots of the deposited liposomes (Figure 6D). These hemichannels were solely from the lipidic membranes on the mica since extensive washing of the sample in the AFM chamber was performed, thus removing any hemichannels in solution prior to this analysis.

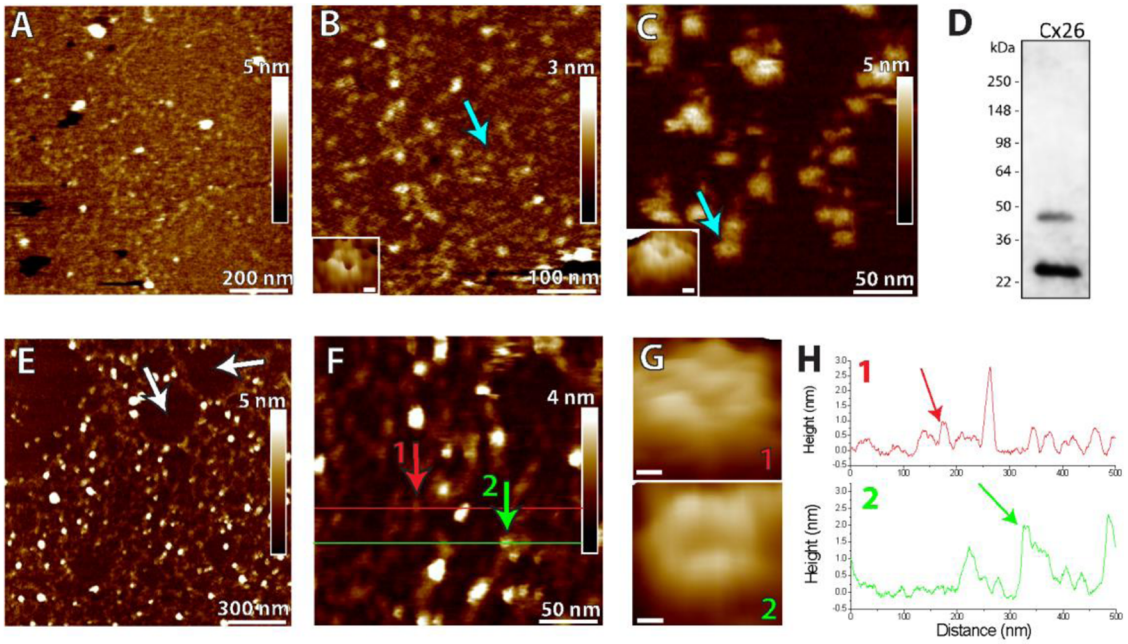

Figure 6. Cx26 hemichannels reconstituted in DOPC liposomes and deposited on mica to form flat membranes. (A–C) Hemichannels were observed in DOPC bilayers with insets showing zoomed images of the hemichannels (location indicated by cyan arrow, scale bar is 2 nm). (D) The presence of Cx26 in the liposomes was confirmed with a Western blot of liposomes deposited on the mica substrate. (E) Membrane patches with no hemichannels present (white arrows) were also observed indicating that some liposomes do not contain hemichannels. (F) Image showing the presence of hemichannels of different heights in the same bilayer. (G) Enlarged images of the channels highlighted in F (scale bar is 2 nm). (H) Cross-sections of the membrane showing the height of the membrane along the lines in F.

dx.doi.org/10.1021/bi501265p | *Biochemistry* 2014, 53, 7407–7414

Not all of the liposomes appeared to contain hemichannels. Some samples showed flat areas where no obvious protrusions were present (Figure 6E). This indicates that the liposomes were not completely saturated with protein. The hemichannels reconstituted into DOPC bilayers displayed two distinct populations of hemichannels based on the protrusion heights (Figure 6F–H). The measured hemichannel heights were fit to multiple Gaussians (Figure 7). The heights of the populations

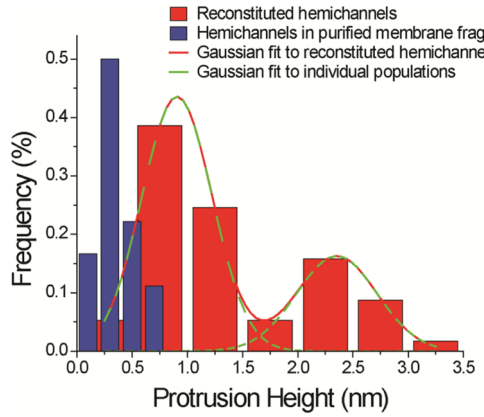

Figure 7. Histograms of protrusion heights of Cx26 hemichannels in purified membrane fragments compared to populations of reconstituted hemichannels. The mean protrusion height of hemichannels in the purified membranes (blue) was lower than for hemichannels reconstituted in DOPC liposomes (red). A Gaussian fit was applied to the two populations of heights observed for reconstituted hemichannels (green line). The protrusion heights were measured as 0.9 ± 0.3 nm and 2.3 ± 0.3 nm reconstituted hemichannels and 0.4 ± 0.2 nm for hemichannels in purified membrane fragments.

based on these fits were measured to be in two groups of 0.9 ± 0.3 nm and 2.3 ± 0.3 nm (n = 58), respectively. Small variations between the heights are most likely due to the influence of the imaging force. The protrusion height of the hemichannels imaged with AFM was statistically significantly greater for the reconstituted hemichannels compared to those imaged in the membranes ($p < 0.01$) (Figure 7).

DISCUSSION

We report for the first time AFM imaging of noncrystalline Cx26 hemichannels in purified membranes expressed through baculovirus infection of insect cells. Preparations of native single (undocked) hemichannel layers isolated from mammalian cells have not been documented, most likely because they are too dispersed in the plasma membrane and do not survive the detergent enrichment. Most reports of single hemichannel layers were from mechanically or chemically split GJs. In addition, the trafficking of GJ channels in native mammalian systems is highly regulated[32] with the caveat that cells maintain only a small number of open hemichannels and subsets of open GJ channels.[33]

Our Sf9 membrane preparations have the advantage of cellular trafficking of hemichannels to the membrane along with guided insertion of hemichannels into the membrane. Consequently, the hemichannels in a single membrane fragment face the same direction in the membrane bilayer (cytoplasmic or extracellular) compared to a random orientation when hemichannels are reconstituted into liposomes. AFM images of purified membrane fragments containing Cx26 hemichannels have patches where the lipid bilayers were thicker. This is likely due to the clustering of hemichannels in the membranes into protein-rich regions. GJ channels are well characterized to form clusters that favor improved interaction energy between cell membranes.[34] In the Owicki model of GJ channel clustering, long-range protein aggregation into GJ plaques arises from interparticle interactions as well as lateral pressures between the junction and the surrounding glycocalyx.[35,36] Whether dense hemichannel packing occurs in internal membrane compartments (ER, Golgi apparatus, trafficking vesicles) has yet to be determined. Normal trafficking of hemichannels occurs through anterograde pathways after which they are fused into the plasma membrane and then coalesce on the edges of GJ plaques where they dock and form GJ plaques.[37,38] Cx26 hemichannels in our present work appear to display aggregating behavior in some of the membranes as the proteins did not appear to be spread homogeneously throughout the membrane. Clustering of ion channels and receptors in single cell plasma membrane is not unusual, and they serve as important communication links between the cells and their surroundings.[39] Large lipidic patches of membrane could be observed (Figures 2, 3) next to the protein-rich regions. The step height between the protein-rich and lipidic membrane regions was 1.8 ± 0.4 nm. This step height is similar to protrusion heights for Cx26 GJ channels measured with EM, X-ray diffraction, and X-ray crystallography. Measurements of protrusion heights obtained from the X-ray crystallographic atomic model were 1.9 nm for the cytoplasmic domains and 2.3 nm for the extracellular domain.[14] It is important to note that this is probably an estimate since these GJ channels were not membrane embedded as well as the protrusion height measurement represented one-half the distance measured for the docked dodecameric GJ channel.

High resolution images of the cytoplasmic domains of the hemichannel were likely to be reduced slightly by the presence of the His_6 and V5 tags on the Cx26 connexins. The presence of terminal tags would increase the floppiness of cytoplasmic side of the hemichannels and could possibly inhibit imaging slightly. The protrusion heights of the hemichannels measured in purified membrane fragments were lower than those previously reported for crystal and quasi-crystalline structures. The heights were likely reduced due to the high density and disorder of the surrounding proteins reducing the true height of the channel compared to its surrounding. The protrusion height of hemichannels in DOPC bilayers was observed to be greater than those found in the membranes with 0.4 ± 0.2 nm for the hemichannels in purified membrane fragments and 0.9 ± 0.3 nm and 2.3 ± 0.3 nm for the two populations of channels observed in reconstituted DOPC membranes. The greater protrusion height observed for the reconstituted proteins is likely a result of the AFM probe being able to access the membrane more easily due to lower hemichannel densities.

The protrusion height of the reconstituted hemichannels showed distinct populations likely due to differences in the cytoplasmic and extracellular structures. The measured protrusion height above the bilayer for the reconstituted channels measured by AFM was 0.9 ± 0.3 nm and 2.3 ± 0.3 nm. Fiber diffraction analysis of pellets containing partially oriented GJs revealed that the extracellular gap between two membranes with GJ channels was ~3.5 nm thick, which would estimate extracellular protrusions of ~1.8 nm.[15] Similar sizes were observed in density maps of Cx26 GJ channels reconstituted into DOPC membranes with extracellular gaps

dx.doi.org/10.1021/bi501265p | Biochemistry 2014, 53, 7407–7414

of ∼4 nm for reconstituted Cx26 in a DOPC membrane (∼2 nm per an extracellular protrusion).[29,40] Measurements of the cytoplasmic tails have been more elusive due to the flexibility of the cytoplasmic tails. In the best structurally preserved part of the three layer structure, the cytoplasmic protrusion heights measured in these EM density maps were ∼2−2.5 nm for Cx26 containing a His_6 tag and a thrombin cleavage site of 6 amino acids, but without a 14 amino acid V5 epitope tag.[29] In addition, this structure was determined at 4 °C temperature, so the assumption is that it would be more rigid under these conditions than in our room temperature AFM imaging chamber. It should also be noted that the X-ray crystallographic data were recorded from crystals flash frozen in liquid nitrogen. We found that, as measured with AFM, the cytoplasmic face of Cx26 hemichannels is highly sensitive to the applied force with decreases in the observed protrusion height from 1.7 nm at 50 pN of force to 0.2 nm at 70 pN in quasi-crystalline packing.[18] Dispersed hemichannel proteins should have increased flexibility allowing the proteins to flatten more easily due to the lack of a lattice structure. The intrinsically high flexibility of the cytoplasmic surfaces and hemichannel dispersion likely accounts for the population height observed for reconstituted hemichannel proteins. The hemichannels with lower protrusions of 0.9 ± 0.3 nm are most likely cytoplasmic while the larger protrusion heights (2.3 ± 0.3 nm) are the extracellular domains, which are more rigid.

We report high resolution AFM imaging of noncrystalline disordered Cx26 hemichannels expressed in membranes for the first time. Previous studies on the structure of hemichannels with AFM have revealed high resolution structures of hemichannels. Images of hemichannels that had been force dissected with AFM have revealed in great detail the structure of extracellular and cytoplasmic domains of hemichannels in quasi-crystalline structures.[18] However, these docked hemichannel systems vary from native hemichannel presentations, which involve formation of disordered hemichannel arrays in the plasma membrane and subsequently aggregate into GJ edges in order to dock.[41] Structures of disordered noncrystalline hemichannels have also been studied in reductionist systems involving reconstituted proteins in lipid bilayers.[20,21] These systems fail to represent the complex environments seen in cellular systems where the proteins are trafficked to a plasma membrane, which contains diverse lipid compositions and other membrane proteins, before the hemichannels freely diffuse to the edge of a GJ.[37,38] The system presented in this paper for AFM imaging allows study of connexin hemichannels in a more complex membrane environment that includes mixed lipid composition and other membrane proteins, which more closely mimics the environment of native cells. The behavior of the Cx26 hemichannels in the purified membrane environment differs from proteoliposomal systems through increased density of channels and apparent aggregation of proteins in the membranes. In addition to showing clustering of properly trafficked connexin hemichannels, this system presents unique opportunities to study the structure of hemichannel proteins and their cooperative behavior using electrophysiological and high resolution imaging with AFM.

AUTHOR INFORMATION

Corresponding Authors

*E-mail: gsosinsky@ucsd.edu.
*E-mail: rlal@ucsd.edu.

Author Contributions

The manuscript was written through contributions of all authors. All authors have given approval to the final version of the manuscript. Gina Sosinsky and Ratnesh Lal laboratories contributed equally to this work.

Funding

National Institute of Health grants R01DA024871 (R.L.), R01DA025296 (R.L.), R01GM065937 (G.S.), and F31DA034562 (B.M.). Some of the work presented here was conducted at the National Center for Microscopy and Imaging Research at San Diego, which is supported by NIH Grant P41GM103412 awarded to Dr. Mark Ellisman.

Notes

The authors declare no competing financial interest.

ACKNOWLEDGMENTS

The authors thank Cynthia Y. Ren for assistance in Western blots and protein staining.

ABBREVIATIONS USED

AFM, atomic force microscopy; Cx, Connexin; GJ, gap junction; DoDM, *n*-dodecyl-*β*-D-maltoside; OG, *n*-octyl-*β*-D-glucoside; Sf9, *Spodoptera frugiperda*; PMSF, phenylmethylsulfonyl fluoride; DOPC, 1,2-dioleoyl-*sn*-glycero-3-phosphatidylcholine; EM, electron microscopy

REFERENCES

(1) Lal, R., John, S. A., Laird, D. W., and Arnsdorf, M. F. (1995) Heart gap junction preparations reveal hemiplaques by atomic force microscopy. *Am. J. Physiol. Cell Physiol. 268*, C968−C977.

(2) Fiori, M. C., Figueroa, V., Zoghbi, M. E., Saéz, J. C., Reuss, L., and Altenberg, G. A. (2012) Permeation of calcium through purified connexin 26 hemichannels. *J. Biol. Chem. 287*, 40826−40834.

(3) Gaßmann, O., Kreir, M., Ambrosi, C., Pranskevich, J., Oshima, A., Röling, C., Sosinsky, G., Fertig, N., and Steinem, C. (2009) The M34A mutant of Connexin26 reveals active conductance states in pore-suspending membranes. *J. Struct. Biol. 168*, 168−176.

(4) Ramachandran, S., Arce, F. T., Patel, N. R., Quist, A. P., Cohen, D. A., Lal, R. (2014) Structure and permeability of ion-channels by integrated AFM and waveguide TIRF microscopy, *Sci. Rep. 4*.

(5) Harris, A. L. (2007) Connexin channel permeability to cytoplasmic molecules. *Prog. Biophys. Mol. Biol. 94*, 120−143.

(6) Li, H., Liu, T.-F., Lazrak, A., Peracchia, C., Goldberg, G. S., Lampe, P. D., and Johnson, R. G. (1996) Properties and regulation of gap junctional hemichannels in the plasma membranes of cultured cells. *J. Cell Biol. 134*, 1019−1030.

(7) Contreras, J. E., Sáez, J. C., Bukauskas, F. F., and Bennett, M. V. L (2003) Gating and regulation of connexin 43 (Cx43) hemichannels. *Proc. Natl. Acad. Sci. U.S.A. 100*, 11388−11393.

(8) Axelsen, L. N., Calloe, K., Holstein-Rathlou, N.-H., Nielsen, M. S. (2013) Managing the complexity of communication: regulation of gap junctions by post-translational modification, *Front. Pharmacol. 4*.

(9) Kondo, R. P., Wang, S.-Y., John, S. A., Weiss, J. N., and Goldhaber, J. I. (2000) Metabolic inhibition activates a non-selective current through connexin hemichannels in isolated ventricular myocytes. *J. Mol. Cell. Cardiol. 32*, 1859−1872.

(10) Paul, D. L., Ebihara, L., Takemoto, L. J., Swenson, K. I., and Goodenough, D. A. (1991) Connexin46, a novel lens gap junction protein, induces voltage-gated currents in nonjunctional plasma membrane of Xenopus oocytes. *J. Cell Biol. 115*, 1077−1089.

(11) Ramachandran, S., Xie, L.-H., John, S. A., Subramaniam, S., and Lal, R. (2007) A novel role for connexin hemichannel in oxidative stress and smoking-induced cell injury. *PLoS One 2*, e712.

(12) Retamal, M. A., Cortés, C. J., Reuss, L., Bennett, M. V. L, and Sáez, J. C. (2006) S-nitrosylation and permeation through connexin 43

hemichannels in astrocytes: induction by oxidant stress and reversal by reducing agents. *Proc. Natl. Acad. Sci. U.S.A. 103*, 4475−4480.
(13) Oshima, A., Tani, K., Hiroaki, Y., Fujiyoshi, Y., and Sosinsky, G. E. (2007) Three-dimensional structure of a human connexin26 gap junction channel reveals a plug in the vestibule. *Proc. Natl. Acad. Sci. U.S.A. 104*, 10034−10039.
(14) Maeda, S., Nakagawa, S., Suga, M., Yamashita, E., Oshima, A., Fujiyoshi, Y., and Tsukihara, T. (2009) Structure of the connexin 26 gap junction channel at 3.5 Ã resolution. *Nature 458*, 597−602.
(15) Makowski, L., Caspar, D. L. D., Phillips, W. C., and Goodenough, D. A. (1977) Gap junction structures: Analysis of the x-ray diffraction data. *J. Cell Biol. 74*, 629−645.
(16) Unger, V. M., Kumar, N. M., Gilula, N. B., and Yeager, M. (1999) Three-dimensional structure of a recombinant gap junction membrane channel. *Science 283*, 1176−1180.
(17) Perkins, G., Goodenough, D., and Sosinsky, G. (1997) Three-dimensional structure of the gap junction connexon. *Biophys. J. 72*, 533−544.
(18) Müller, D. J., Hand, G. M., Engel, A., and Sosinsky, G. E. (2002) Conformational changes in surface structures of isolated connexin 26 gap junctions. *EMBO J. 21*, 3598−3607.
(19) Yu, J., Bippes, C. A., Hand, G. M., Muller, D. J., and Sosinsky, G. E. (2007) Aminosulfonate modulated pH-induced conformational changes in connexin26 hemichannels. *J. Biol. Chem. 282*, 8895−8904.
(20) Thimm, J., Mechler, A., Lin, H., Rhee, S., and Lal, R. (2005) Calcium-dependent open/closed conformations and interfacial energy maps of reconstituted hemichannels. *J. Biol. Chem. 280*, 10646−10654.
(21) Allen, M. J., Gemel, J., Beyer, E. C., and Lal, R. (2011) Atomic force microscopy of Connexin40 gap junction hemichannels reveals calcium-dependent three-dimensional molecular topography and open-closed conformations of both the extracellular and cytoplasmic faces. *J. Biol. Chem. 286*, 22139−22146.
(22) Sorgen, P. L., Duffy, H. S., Sahoo, P., Coombs, W., Delmar, M., and Spray, D. C. (2004) Structural changes in the carboxyl terminus of the gap junction protein connexin43 indicates signaling between binding domains for c-Src and zonula occludens-1. *J. Biol. Chem. 279*, 54695−54701.
(23) Pfenniger, A., Wohlwend, A., and Kwak, B. R. (2011) Mutations in connexin genes and disease. *Eur. J. Clin. Invest. 41*, 103−116.
(24) Ambrosi, C., Walker, A. E., DePriest, A. D., Cone, A. C., Lu, C., Badger, J., Skerrett, I. M., and Sosinsky, G. E. (2013) Analysis of trafficking, stability and function of human connexin 26 gap junction channels with deafness-causing mutations in the fourth transmembrane helix. *PLoS One 8*, e70916.
(25) Xu, J., and Nicholson, B. J. (2013) The role of connexins in ear and skin physiology-functional insights from disease-associated mutations. *Biochim. Biophys. Acta 1828*, 167−178.
(26) Beahm, D. L., Oshima, A., Gaietta, G. M., Hand, G. M., Smock, A. E., Zucker, S. N., Toloue, M. M., Chandrasekhar, A., Nicholson, B. J., and Sosinsky, G. E. (2006) Mutation of a conserved threonine in the third transmembrane helix of α-and β-connexins creates a dominant-negative closed gap junction channel. *J. Biol. Chem. 281*, 7994−8009.
(27) Ambrosi, C., Boassa, D., Pranskevich, J., Smock, A., Oshima, A., Xu, J., Nicholson, B. J., and Sosinsky, G. E. (2010) Analysis of four connexin26 mutant gap junctions and hemichannels reveals variations in hexamer stability. *Biophys. J. 98*, 1809−1819.
(28) Ambrosi, C., Gassmann, O., Pranskevich, J. N., Boassa, D., Smock, A., Wang, J., Dahl, G., Steinem, C., and Sosinsky, G. E. (2013) Pannexin1 and Pannexin2 channels show quaternary similarities to connexons and different oligomerization numbers from each other. *J. Biol. Chem. 285*, 24420−24431.
(29) Oshima, A., Tani, K., Toloue, M. M., Hiroaki, Y., Smock, A., Inukai, S., Cone, A., Nicholson, B. J., Sosinsky, G. E., and Fujiyoshi, Y. (2011) Asymmetric configurations and N-terminal rearrangements in connexin26 gap junction channels. *J. Mol. Biol. 405*, 724−735.
(30) Hand, G. M., Müller, D. J., Nicholson, B. J., Engel, A., and Sosinsky, G. E. (2002) Isolation and characterization of gap junctions from tissue culture cells. *J. Mol. Biol. 315*, 587−600.
(31) Leonenko, Z. V., Finot, E., Ma, H., Dahms, T. E. S., and Cramb, D. T. (2004) Investigation of temperature-induced phase transitions in DOPC and DPPC phospholipid bilayers using temperature-controlled scanning force microscopy. *Biophys. J. 86*, 3783−3793.
(32) Musil, L. S., Le, A.-C. N., VanSlyke, J. K., and Roberts, L. M. (2000) Regulation of connexin degradation as a mechanism to increase gap junction assembly and function. *J. Biol. Chem. 275*, 25207−25215.
(33) Bukauskas, F. F., Jordan, K., Bukauskiene, A., Bennett, M. V. L, Lampe, P. D., Laird, D. W., and Verselis, V. K. (2000) Clustering of connexin 43-enhanced green fluorescent protein gap junction channels and functional coupling in living cells. *Proc. Natl. Acad. Sci. U.S.A. 97*, 2556−2561.
(34) Bruinsma, R., Goulian, M., and Pincus, P. (1994) Self-assembly of membrane junctions. *Biophys. J. 67*, 746−750.
(35) Abney, J. R., Braun, J., and Owicki, J. C. (1987) Lateral interactions among membrane proteins. Implications for the organization of gap junctions. *Biophys. J. 52*, 441−454.
(36) Braun, J., Abney, J. R., and Owicki, J. C. (1984) How a gap junction maintains its structure. *Nature 310*, 316−318.
(37) Baker, S. M., Buckheit, R. W., and Falk, M. M. (2010) Green-to-red photoconvertible fluorescent proteins: tracking cell and protein dynamics on standard wide-field mercury arc-based microscopes. *BMC Cell Biol. 11*, 15.
(38) Lauf, U., Giepmans, B. N. G., Lopez, P., Braconnot, S. b., Chen, S.-C., and Falk, M. M. (2002) Dynamic trafficking and delivery of connexons to the plasma membrane and accretion to gap junctions in living cells. *Proc. Natl. Acad. Sci. U.S.A. 99*, 10446−10451.
(39) Lal, R., and Yu, L. (1993) Atomic force microscopy of cloned nicotinic acetylcholine receptor expressed in Xenopus oocytes. *Proc. Natl. Acad. Sci. U.S.A. 90*, 7280−7284.
(40) Rico, F., Oshima, A., Hinterdorfer, P., Fujiyoshi, Y., and Scheuring, S. (2011) Two-dimensional kinetics of inter-connexin interactions from single-molecule force spectroscopy. *J. Mol. Biol. 412*, 72−79.
(41) Johnson, R., Hammer, M., Sheridan, J., and Revel, J.-P. (1974) Gap junction formation between reaggregated Novikoff hepatoma cells. *Proc. Natl. Acad. Sci. U.S.A. 71*, 4536−4540.